

# Electrochemistry and catalytic behavior of immobilized binuclear complexes of copper(II) and nickel(II) with Robson type ligand

Nataliya V. Roznyatovskaya ·  
Veronika K. Laurinavichute · Galina A. Tsirlina ·  
Vladimir M. Mirsky

Received: 13 July 2006 / Revised: 5 October 2006 / Accepted: 18 October 2006 / Published online: 14 December 2006  
© Springer-Verlag 2006

**Abstract** Various systems containing immobilized binuclear copper(II) and nickel(II) complexes with Robson type ligand ( $[M_2L]Cl_2$ ) are studied and compared in relation to catalysis of hydrogen peroxide reduction. Molecular complexes adsorbed on mercury and gold, crystalline complexes immobilized in the carbon paste electrode, and complex species entrapped into polyphenol-modified gold electrodes are considered. Electrocatalysis is assumed to result from the formation of  $H_2O_2-[M_2L]Cl_2$  adduct, not from mediating redox transformations. Possible geometry of the formed reaction layers supporting adduct formation is discussed.

**Keywords** Binuclear copper macrocyclic complex · Cyclic voltammetry · Adsorption · Carbon paste electrodes · Electroreduction

## Introduction

Metalloporphyrins and metallophthalocyanines are well known as effective electrocatalysts for oxygen reduction [1, 2]. This reaction proceeds with the hydrogen peroxide

or water formation in dependence on the mechanism and structure of electrocatalyst molecule.

The four-electron reduction of  $O_2$  has been in particular achieved using dicobalt cofacial porphyrin dimers [3, 4] and phthalocyanine dimers [5]. Another interesting example of four-electron  $O_2$  reduction catalyst is the planar binuclear macrocyclic cobalt complex adsorbed on graphite [2]. These catalysts present the examples of configuration with a certain distance between two metal atoms favoring simultaneous interaction of the  $O_2$  or  $H_2O_2$  molecule with two centers and the resulting high reactivity of adduct. Some water-soluble phthalocyanines are reported to form  $-O-O-$  bridged dimeric complexes in aqueous electrolytes [2].

Through the example of cobalt face-to-face porphyrin dimer [4, 6] the optimal metal–metal distance should be close to 4 Å for effective catalysis of  $O_2$  reduction with bond rupture. The authors propose that the formation of  $Co-O-O-Co$  bridge between two Co centers located at this distance from each other favors the rupture of the  $-O-O-$  bond. Generally, there are two ways to make two metal (catalytic) centers in close proximity: either to design a ligand containing two compartments to coordinate two metal ions, or to draw two mononuclear molecules nearby in such a way that two metal centers of these molecules should be at a short distance from each other.

The binuclear Robson-type complexes are analogous to porphyrins (or phthalocyanines) because of their quasiplanar geometry and  $\pi$ -conjugated electronic system. These complexes have already manifested the activity in binding CO [7] and in catalysis of  $H_2O_2$  disproportionation [8], but rarely tested as electrocatalysts. The distance between two metal centers in Robson-type complexes (ca. 3 Å) is probably too short to bind both oxygen atoms of  $H_2O_2$ . However, it may be possible to realize an assembly of

N. V. Roznyatovskaya (✉) · V. K. Laurinavichute · G. A. Tsirlina  
Department of Electrochemistry, Faculty of Chemistry,  
Moscow State University,  
Leninskie Gory 1-str.3,  
Moscow 119992, Russia  
e-mail: natasha@elch.chem.msu.ru

V. M. Mirsky  
Institute of Analytical Chemistry, Chemo- and Biosensors,  
University of Regensburg,  
Universitätstrasse 31,  
93040 Regensburg, Germany

molecules with slightly longer metal–metal distance in adsorption layer directly at the electrode surface.

The aim of this study is to clarify the nature of  $[M_2L]Cl_2$  ( $M=Cu, Ni$ , Fig. 1) effect on  $H_2O_2$  reduction and to arrange this catalysis at solid electrodes modified by  $[M_2L]Cl_2$ . By these means, we continue our studies of  $[M_2L]Cl_2$  aqueous electrochemistry [9–11] including the first observation of  $H_2O_2$  electrocatalysis by  $[Ni_2L]Cl_2$  at mercury electrode. At this subsequent stage, we attempt to clarify the reasons of electrocatalytic behavior in dependence on the nature of the central atom and the state of immobilized complex. The latter is varied below from adsorbed to fixed in two different 3D configurations (polymer-linked and crystalline).

## Experimental

### Chemicals

$CH_3COON \cdot 3H_2O$ , glacial acetic acid, and NaCl (pure per analysis, Merck) were used for preparation of supporting solution. Demineralized water used to prepare solutions was additionally purified by passing it through a Millipore-Milli-Q system, the final resistivity being at least  $18 M\Omega \text{ cm}$ .

Methanol, ethanol, and hexane were Merck reagents (pure per analysis), 60% teflon suspension in water was purchased from Aldrich, and carbon powder (Vulcan X1-72R,  $272 \text{ m}^2/\text{g}$ ) from Cabot. These chemicals were used to prepare carbon paste electrodes.

$[Cu_2L]Cl_2 \cdot H_2O$  and  $[Ni_2L]Cl_2 \cdot 2H_2O$  were prepared and characterized following literature method [13]. Analytical data for  $[Cu_2L]Cl_2 \cdot H_2O$  were reported previously in [10].

Phenol was twice recrystallized from water. The working solutions of  $H_2O_2$  were prepared by dilution of 30%  $H_2O_2$  (Fluka). The concentration of diluted stock  $H_2O_2$  solution was precised by permanganatometric titration.

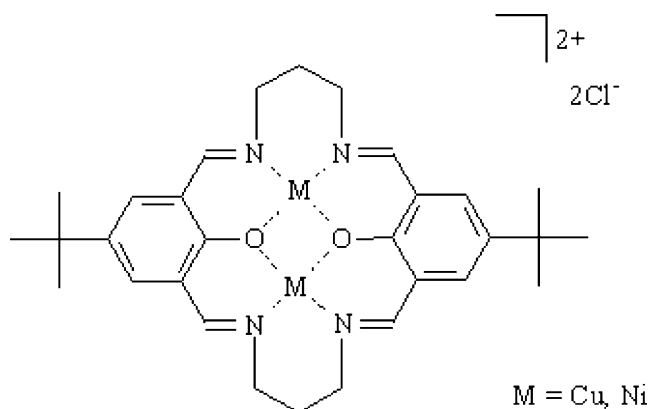


**Fig. 1** Schematic structure of  $[Cu_2L]Cl_2$  and  $[Ni_2L]Cl_{2a}$

### Instrumentation

Cyclic voltammograms were recorded using either EG&G PARC 273A potentiostat/galvanostat or Autolab PGSTAT 10 controlled by software running on a PC. The measurements were carried out in a three-electrode glass cell with separated compartments using a saturated calomel electrode (SCE) as the reference connected with a cell via Luggin capillary with saturated KCl salt bridge, and a Pt plate as the auxiliary electrode.

All potentials below are referred to SCE. Surface plasmon resonance (SPR) measurements were performed on a SPR-spectrometer BIOSUPLAR-321 (Mivitec GmbH-Analytical  $\mu$ -Systems) with a two-channel flow cell. The construction provided differential measurements and corresponding correction of temperature fluctuations. The flow rate was  $40 \text{ ml s}^{-1}$ . The 50 nm gold films, thermally evaporated onto 1 mm thick glass slides of refractive index 1.61 (the same supplier) with chromium adhesive sublayer were used.

### Immobilization procedures

#### Carbon paste electrodes

The preparation of carbon paste electrodes (CPE) modified with  $[Cu_2L]Cl_2$  and  $[Ni_2L]Cl_2$  included several steps (*procedure 1*). A 2.7 mg of  $[Cu_2L]Cl_2$  or  $[Ni_2L]Cl_2$  with carbon powder (5.3 mg) ( $w/w$  1:2) was slurried in a mixture of 200  $\mu\text{l}$  of hexane, 100  $\mu\text{l}$  of ethanol, and 20  $\mu\text{l}$  of preliminary diluted teflon suspension (20  $\mu\text{l}$  of 60% suspension for 400  $\mu\text{l}$  of water). The suspension was sonicated during 30 min for homogenization. Then, the solvents were evaporated in the stream of argon. The final slurried carbon mass was mechanically traced onto thin film gold electrodes (700  $\mu\text{m}$  diameter) on Si/SiO<sub>2</sub> support and slightly pressed to establish electrical contact.

The electrodes with a weight ratio  $[Cu_2L]Cl_2$ /carbon powder of 1:1, 1:2, and 2:1 were fabricated and tested. Blank carbon paste electrode was prepared in a way described above taking 8 mg of carbon powder.

In the case of  $[Cu_2L]Cl_2$ , slightly different procedure (*procedure 2*) was also applied. The paste was prepared by sonication of mixture of 2 mg  $[Cu_2L]Cl_2$ , 6 mg carbon powder, 700  $\mu\text{l}$  ethanol, and 20  $\mu\text{l}$  preliminary diluted teflon suspension (20  $\mu\text{l}$  of 60% for 400  $\mu\text{l}$  of water) for 20 min. Then, 20  $\mu\text{l}$  portion of this mixture was deposited onto gold surface and dried at room temperature.

#### Polyphenol modified electrodes

The immobilization of the metal complexes with organic ligand into polymer films requires usually mild condition of polymerization. Polyphenol is formed by electrooxidation

of phenol by cycling potential with anodic limit ca. +1 V [12]. To prepare electrodes modified by polyphenol films, an electropolymerization under cyclic voltammetric mode was carried out on a gold wire electrodes (geometric surface is ca. 0.07 cm<sup>2</sup>) in solution of monomer (3 mM) in acetate buffer (pH 6). Before modification, the gold wire electrodes were chemically etched as the electrodes prepared for electrochemical measurements.

Preliminary tests for possible [M<sub>2</sub>L]Cl<sub>2</sub> oxidation were carried out with [Cu<sub>2</sub>L]Cl<sub>2</sub> in the absence of phenol and demonstrated no redox activity of [Cu<sub>2</sub>L]Cl<sub>2</sub> in the potential range from -0.2 to 1 V.

The polymerization of phenol with addition of [Cu<sub>2</sub>L]Cl<sub>2</sub> was observed under potential cycling between -0.2 and 0.7 V. Fast decrease of anodic current (up to the value in supporting electrolyte) was registered during polymerization. The thickness of the film was estimated to be ca. 8 nm for polymerization without [Cu<sub>2</sub>L]Cl<sub>2</sub> and ca. 5–10 in the presence of [Cu<sub>2</sub>L]Cl<sub>2</sub>, the potential was cycled between -0.2 and 0.7 V.

To prove if the complexes are incorporated into the film, an XPS analysis (X-ray Photoelectron Spectroscopy) was carried out. It was shown that [Ni<sub>2</sub>L]Cl<sub>2</sub> is not included into film while [Cu<sub>2</sub>L]Cl<sub>2</sub> is incorporated but loses its redox activity. This electrode is denoted in this study as PP-[Cu<sub>2</sub>L]Cl<sub>2</sub>-Au.

Test for H<sub>2</sub>O<sub>2</sub> decomposition under experimental conditions

One cannot exclude that the observed effects result from homogeneous H<sub>2</sub>O<sub>2</sub> decomposition with subsequent electrochemical consumption of radicals, or from potential-independent heterogeneous decomposition. Therefore, it is important to get the evidence of electrocatalytic nature of the phenomena in [M<sub>2</sub>L]Cl<sub>2</sub>-based systems.

To ensure that the modified electrodes do not assist decomposition of H<sub>2</sub>O<sub>2</sub>, the following test was taken. Both modified and bare electrodes were immersed into H<sub>2</sub>O<sub>2</sub> solution. The decrease of H<sub>2</sub>O<sub>2</sub> concentration was more than 3% for 20 h according to the titration data. The addition of [Cu<sub>2</sub>L]Cl<sub>2</sub> (1·10<sup>-4</sup> M) to the H<sub>2</sub>O<sub>2</sub> solution do not induce any change of H<sub>2</sub>O<sub>2</sub> concentration. Therefore, the (catalytic) decomposition of H<sub>2</sub>O<sub>2</sub> hardly interferes the electrocatalytic reduction of H<sub>2</sub>O<sub>2</sub>.

To test whether the catalytic feature of [Ni<sub>2</sub>L]Cl<sub>2</sub> is caused by adsorbed or dissolved [Ni<sub>2</sub>L]Cl<sub>2</sub> species (the H<sub>2</sub>O<sub>2</sub> binding to [Ni<sub>2</sub>L]Cl<sub>2</sub> takes place at the electrode surface), the solution of [Ni<sub>2</sub>L]Cl<sub>2</sub> was studied by UV-Vis spectroscopy. No [Ni<sub>2</sub>L]Cl<sub>2</sub> spectrum change was observed after addition of H<sub>2</sub>O<sub>2</sub>. Consequently, the [Ni<sub>2</sub>L]Cl<sub>2</sub>-H<sub>2</sub>O<sub>2</sub> adduct, if any, is more likely formed at the electrode surface.

Measurement procedures

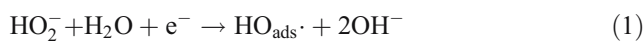
All solutions for CV experiments were supported with acetate buffer (0.1 or 0.05 M, pH 6.0) and were deaerated with argon during at least 25 min before measurements. Before measurements, the gold wire electrode was pre-treated with a hot mixture of concentrated nitric and hydrochloric acids (1:3) and rinsed thoroughly with deionized water.

Dropping mercury electrode (flow rate of 0.84 mg s<sup>-1</sup>; open circuit drop life time 7.8 s) was used to measure drop life time vs potential in solutions of [Ni<sub>2</sub>L]Cl<sub>2</sub> (pH 6). The surface tension of the mercury-solution interface was calculated from the drop lifetime values by calibration with equilibrium electrocapillary curve in the background solution (0.1 M acetate buffer, pH 6). Data processing of the drop lifetime vs potential and concentration dependencies was performed by conventional procedure for surface active substances [14]. Distance estimation between the neighboring [M<sub>2</sub>L]Cl<sub>2</sub> molecules in adsorption layer was based on [M<sub>2</sub>L]Cl<sub>2</sub> crystallographic data.

## Results and discussion

Mechanisms of H<sub>2</sub>O<sub>2</sub> reduction

Pyrographite, gold, and mercury electrodes demonstrate low activity towards hydrogen peroxide reduction [15]. The key stages of H<sub>2</sub>O<sub>2</sub> reduction at these electrodes are [16, 18]:



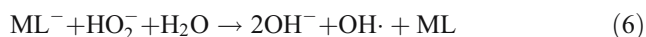
where HO<sub>ads</sub>· is hydroxyl radical adsorbed at the electrode surface, and the reaction (1) with bond rupture is the limiting step.

At the electrode surfaces modified by a metal complex ML, H<sub>2</sub>O<sub>2</sub> electrocatalytic reduction implies either the crucial role of redox reaction of the central metal atom of the catalyst, or an activation of -O-O- bond by binding of H<sub>2</sub>O<sub>2</sub> molecule. For the modifier ML, the former mechanism is typically presented as:



The first step involves an interaction of HO<sub>2</sub><sup>-</sup> with ML (Eq. 3), then a charge transfer (Eq. 4) followed by O-O bond rupture and protonation occurs.

An alternative mechanism based on redox catalysis includes mediator reduction (Eq. 5) followed by chemical reaction of hydrogen peroxide with reduced mediator (Eq. 6):



Detailed elaboration of this mechanism was reported for a number of mononuclear complexes (see e.g., [17]).

$[\text{Cu}_2\text{L}]\text{Cl}_2$  is redox active in a wide potential range [11]. Therefore, its hypothetical effect on  $\text{H}_2\text{O}_2$  electroreduction is possible according to both Eqs. 2, 3 and Eqs. 5, 6 via adduct formation and a mediator mechanism. For mercury electrode, a slight inhibition by  $[\text{Cu}_2\text{L}]\text{Cl}_2$  was observed, and its reasons are also of interest for our analysis. At the same time, only the mechanism of adduct formation (Eqs. 3, 4) can be expected for  $[\text{Ni}_2\text{L}]\text{Cl}_2$  because of its redox inactivity in the potential region where  $\text{H}_2\text{O}_2$  electrocatalysis on mercury was observed [9].

Unfortunately, there is no detailed mechanistic information concerning  $\text{H}_2\text{O}_2$  reduction in neutral and weakly acidic media. Available information requires assuming an important role of  $\text{OH}^-$  adsorption on gold. As the catalytic effects discussed below are not extremely high, one should take into account possible interplay of schemes (2) or/and (3) with scheme (1) for pure metal. This problem is closely related to analysis of adsorption phenomena in the presence of catalysts.

Compared to metalloporphyrins and phthalocyanines, there are two potential catalytic sites in  $[\text{M}_2\text{L}]\text{Cl}_2$  ( $\text{M}=\text{Cu}, \text{Ni}$ ). Therefore, if the catalysis of  $\text{H}_2\text{O}_2$  electroreduction is considered, one can expect not only mechanism involving radical formation (Eq. 5), but also a parallel two-electron transfer when  $\text{HO}_2^-$  interacts with two sites simultaneously.

Dissolved  $[\text{Ni}_2\text{L}]\text{Cl}_2$ ,  $[\text{Cu}_2\text{L}]\text{Cl}_2 + \text{H}_2\text{O}_2$

Electrocatalysis of  $\text{H}_2\text{O}_2$  in the presence of strongly adsorbed  $[\text{Ni}_2\text{L}]\text{Cl}_2$  was found earlier at a mercury electrode [9]. In this section, we are focused on a search of a similar effect on solid electrodes represented by polycrystalline gold as a model system.  $[\text{Cu}_2\text{L}]\text{Cl}_2$  is redox active on gold starting from  $-0.4$ – $-0.5$  V, and its reduction is chemically irreversible, i.e., there is no difference of reduction onset for gold and mercury electrodes [11].

Dashed curves in Figs. 2 and 3 show cyclic voltammograms of gold wire electrode in  $\text{H}_2\text{O}_2$  solution in acetate buffer solution, pH 6. Solid curve in Fig. 2 demonstrates that  $\text{H}_2\text{O}_2$  reduction current increases in the presence of  $[\text{Cu}_2\text{L}]\text{Cl}_2$  in the potential range from  $-0.2$  to  $-0.5$  V, i.e., only under conditions of  $[\text{Cu}_2\text{L}]\text{Cl}_2$  redox inactivity. This

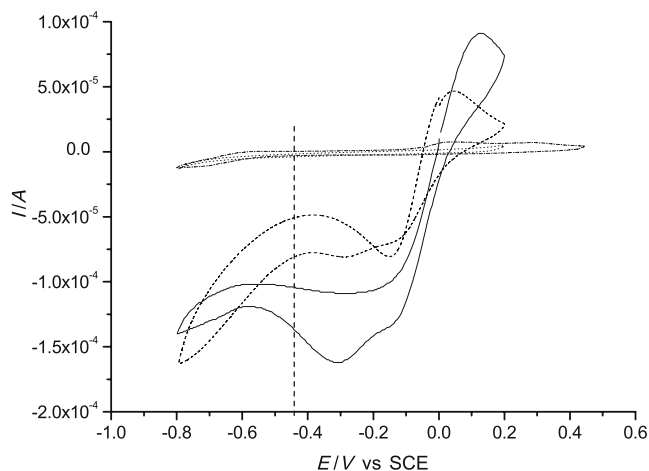


**Fig. 2** Cyclic voltammograms of blank gold wire electrode (the third scans are presented) in 0.01 M acetate buffer solution pH 6.0+ $[\text{Cu}_2\text{L}]\text{Cl}_2$   $x$  mM+ $\text{H}_2\text{O}_2$   $y$  mM, where  $x, y=0, 0$  (dotted line); 0.3, 0 (dash-dotted line); 0, 14 (dashed line); 0.3, 14 (solid line); scan rate 50 mV/s. Vertical dashed line separates the region of  $[\text{Cu}_2\text{L}]\text{Cl}_2$  reduction

potential region is easily available on mercury, but no catalytic effect is observed [9]. The qualitative difference of the surface states of gold and mercury electrodes consists in different sign of the surface charge at potentials more positive than  $-0.5$ : gold is already negatively charged, favoring the adsorption of cationic complex [19].

$[\text{Cu}_2\text{L}]\text{Cl}_2$  reduction current (dash dotted curve in Fig. 2) is low enough as compared to  $\text{H}_2\text{O}_2$  reduction current. The concentrations of  $[\text{Cu}_2\text{L}]\text{Cl}_2$  and  $\text{H}_2\text{O}_2$  were chosen to minimize contribution of complex reduction.

Similarity of  $[\text{Cu}_2\text{L}]\text{Cl}_2$ – $\text{H}_2\text{O}_2$  behavior at mercury and gold is observed at potentials more negative than  $-0.6$ – $-0.8$ : at Hg electrode, polarograms show a pit, that is an inhibition of  $[\text{Cu}_2\text{L}]\text{Cl}_2$  reduction; the current in the

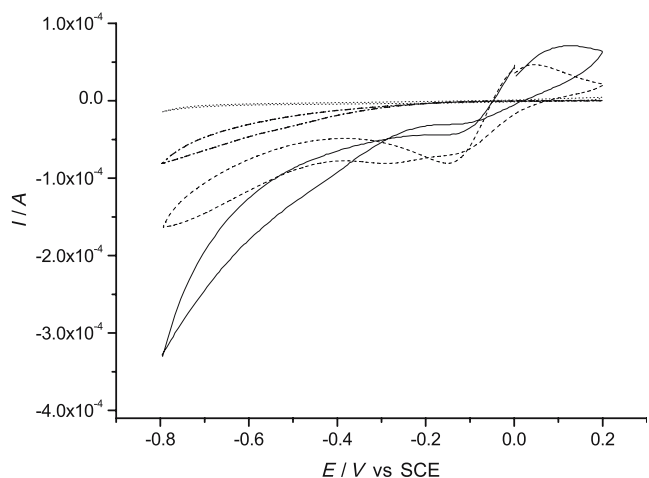
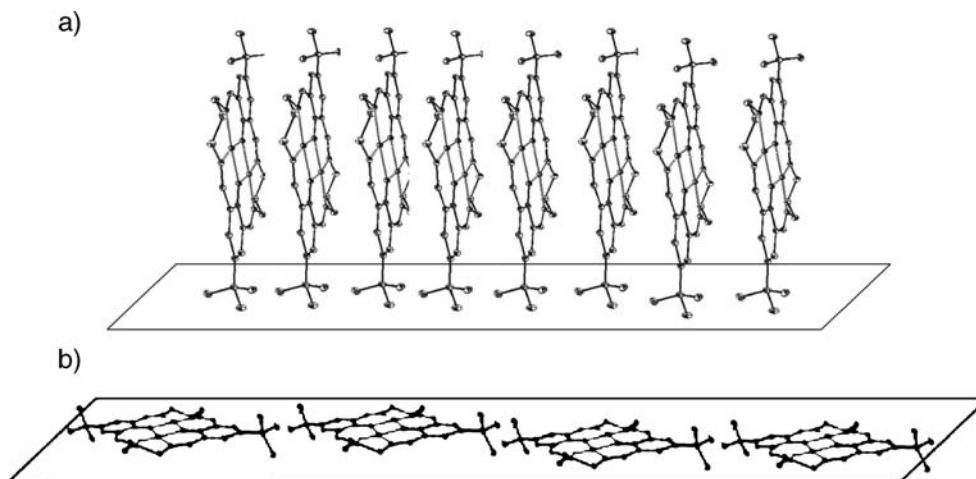


**Fig. 3** Cyclic voltammograms of blank gold wire electrode (the third scans are presented) in 0.01 M acetate buffer solution pH 6.0+ $[\text{Ni}_2\text{L}]\text{Cl}_2$   $x$  mM+ $\text{H}_2\text{O}_2$   $y$  mM, where  $x, y=0, 0$  (dotted line); 0.3, 0 (dash-dotted line); 0, 14 (dashed line); 0.3, 14 (solid lines, arrow denotes consequent cycles from first to sixth); scan rate 50 mV/s

**Fig. 4** Configuration of adsorption layers of  $[\text{Ni}_2\text{L}]\text{Cl}_2$  on mercury electrode



mixture of  $[\text{Cu}_2\text{L}]\text{Cl}_2$  and  $\text{H}_2\text{O}_2$  at gold electrode is equal or lower than the current of  $\text{H}_2\text{O}_2$  reduction in that region (Fig. 2), i.e., inhibition also takes place.

Consequently,  $[\text{Cu}_2\text{L}]\text{Cl}_2$  shows catalytic effect on  $\text{H}_2\text{O}_2$  reduction only if  $[\text{Cu}_2\text{L}]\text{Cl}_2$  has not been reduced, i.e., the scheme (3) is excluded while the scheme (2) is possible. The difference in  $[\text{Cu}_2\text{L}]\text{Cl}_2$  electrocatalytic behavior at mercury and gold at less negative potentials stimulates a search for the difference in adsorption behavior on these metals.

After addition of  $[\text{Ni}_2\text{L}]\text{Cl}_2$  to the  $\text{H}_2\text{O}_2$  solution, the shape of cyclic voltammograms is changed during subsequent cycling, but finally the currents do not exceed the currents of  $\text{H}_2\text{O}_2$  reduction in the potential region more positive than  $-0.3$  V. In the range from  $-0.8$  to  $-0.3$ , a slight increase of  $\text{H}_2\text{O}_2$  reduction current in the presence of  $[\text{Ni}_2\text{L}]\text{Cl}_2$  is observed<sup>1</sup>.

The catalytic effect of  $[\text{Ni}_2\text{L}]\text{Cl}_2$  on  $\text{H}_2\text{O}_2$  reduction at gold electrode is less pronounced than that observed at mercury electrode. Surely, no inhibition of  $\text{H}_2\text{O}_2$  reduction is observed at potentials more negative than  $-0.2$  V; starting from  $-0.5$  V, the current in mixed solution becomes slightly higher than the sum of currents in  $[\text{Ni}_2\text{L}]\text{Cl}_2$  and  $\text{H}_2\text{O}_2$  solutions.

We present below the comparison of adsorption behavior of  $[\text{M}_2\text{L}]\text{Cl}_2$  ( $\text{M}=\text{Cu}, \text{Ni}$ ) at both electrodes and an attempt to estimate the electrode surface coverages by  $[\text{Ni}_2\text{L}]\text{Cl}_2$  or  $[\text{Cu}_2\text{L}]\text{Cl}_2$ .

Due to its redox inactivity at mercury electrode in a wide potential range  $[\text{Ni}_2\text{L}]\text{Cl}_2$  provides a possibility to study adsorption by means of measuring the surface tension. According to these data [9],  $[\text{Ni}_2\text{L}]\text{Cl}_2$  is a strongly adsorbing cation at a mercury–acetate buffer solution

<sup>1</sup> Very low cathodic currents (dash-dotted line Fig. 3) starting from  $-0.3$  V can be hardly interpreted as  $[\text{Ni}_2\text{L}]\text{Cl}_2$  redox activity in this region and can be related to the catalytic reduction of the traces of oxygen by analogy with electroreduction of  $[\text{Ni}_2\text{L}]\text{Cl}_2$  at mercury electrode [9].

interface. Calculated surface excess ( $\Gamma$ ) indicates that high surface coverages ( $\theta$ ) are attained even at submillimolar concentrations of  $[\text{Ni}_2\text{L}]\text{Cl}_2$ . Estimated limiting Gibbs excess  $\Gamma_{\text{max}}$  corresponds to the molecular area of  $0.4 \cdot 10^{-18} \text{ m}^2$ .

To estimate  $\theta$ , we considered two possible limiting configurations of  $[\text{Ni}_2\text{L}]\text{Cl}_2$  in adsorption layer (Fig. 4a,b) using  $[\text{Ni}_2\text{L}]\text{Cl}_2$  geometry extracted from crystal chemistry data (Roznyatovskiy et al., unpublished results). We obtained an area of  $0.4 \cdot 10^{-18} \text{ m}^2$  per molecule for a closely packed (vertical) arrangement (Fig. 4a) and  $1.4 \cdot 10^{-18} \text{ m}^2$  for a flat orientation of  $[\text{Ni}_2\text{L}]\text{Cl}_2$  on electrode surface (Fig. 4b). The former version agrees well with experimental values obtained from processing of electrocapillary measurements. So, when constructing the dependencies of the surface coverage on  $[\text{Ni}_2\text{L}]\text{Cl}_2$ , concentration and potential (Fig. 5) were calculated  $\theta = \frac{\Gamma}{\Gamma_{\text{max}}}$  by using  $\Gamma_{\text{max}}$  for configuration shown in Fig. 4a. This is true at least at

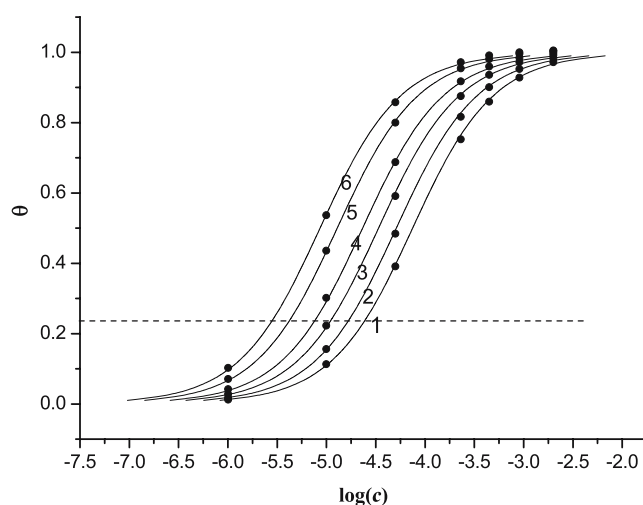


**Fig. 5** Isotherms of  $[\text{Ni}_2\text{L}]\text{Cl}_2$  adsorption on mercury electrode at potentials: (curve 1) 0.4, (2) 0.5, (3) 0.6, (4) 0.7, (5) 0.8, (6) 0.9 V (pH 6, 0.1 M acetate buffer solution). Configuration given in Fig. 3a is assumed. Dashed line corresponds to complete surface coverage for flat configuration (Fig. 3b)

negative electrode charge or  $[\text{Ni}_2\text{L}]\text{Cl}_2$  concentrations above 0.03 mM, i.e., under conditions of electrocatalysis manifestation at mercury.

We assume that the  $[\text{Ni}_2\text{L}]\text{Cl}_2$  closely packed layer on the electrode surface can support  $\text{H}_2\text{O}_2$ – $[\text{Ni}_2\text{L}]\text{Cl}_2$  adduct formation. The distance between nickel(II) atoms of neighboring  $[\text{Ni}_2\text{L}]\text{Cl}_2$  molecules (Fig. 4a) is roughly estimated as ca. 4 Å, favoring dioxygen binding by analogy with (face-to-face) cobalt biporphyrin [6] with the same distance between two metal centers. In contrast, the adlayer structure in Fig. 3b, expected at lower surface coverage (less than 0.25), corresponds to the distance between metal atoms in neighboring molecules above 10 Å when a fixed distance between two nickel centers in the macrocycle is of 3 Å, being too long and too short, respectively, for bridging –O–O– specie. This is a qualitative explanation why the high electrode surface coverage by  $[\text{Ni}_2\text{L}]\text{Cl}_2$  is necessary to obtain the catalytic effect.

As the adsorption of  $[\text{Ni}_2\text{L}]\text{Cl}_2$  on mercury electrode (described above) really looks to be a key phenomenon for electrocatalysis, one shall assign the difference in observed catalytic effect of  $[\text{Ni}_2\text{L}]\text{Cl}_2$  and  $[\text{Cu}_2\text{L}]\text{Cl}_2$  on  $\text{H}_2\text{O}_2$  reduction at mercury to the difference in surface coverage attainable in the solution of  $[\text{Ni}_2\text{L}]\text{Cl}_2$  and  $[\text{Cu}_2\text{L}]\text{Cl}_2$ . In accordance to our polarographic data on electroreduction of  $[\text{Cu}_2\text{L}]\text{Cl}_2$  in the presence of  $[\text{Ni}_2\text{L}]\text{Cl}_2$  (that is reduction under competitive adsorption of these complexes), the adsorption of  $[\text{Cu}_2\text{L}]\text{Cl}_2$  at mercury electrode surface is weaker than that of  $[\text{Ni}_2\text{L}]\text{Cl}_2$  for the same potential window.

Fitting the experimental data obtained on mercury surface (Fig. 5, points) to Frumkin isotherm (Fig. 5, solid curves) (Eq. 7) gives the adsorption equilibrium constant in the range from  $1.2 \cdot 10^5$  to  $1.1 \cdot 10^6$  (increasing systematically with negative potential) and the pronounced dependence of bonding on the electrode charge:

$$B \cdot c = \frac{\theta}{1 - \theta} \cdot e^{-2a\theta} \quad (7)$$

where  $a$ —attraction constant and  $B$ —equilibrium constant.

An attraction constant is found to be ca. 0.1, indicating a weak attraction of adsorbed  $[\text{Ni}_2\text{L}]\text{Cl}_2$  species.

On the basis of indirect data, we suspected earlier the adsorption of  $[\text{Cu}_2\text{L}]\text{Cl}_2$  on gold support [9]. To clarify the main trends related to electrocatalysis, we performed experiments by surface plasmon resonance technique (SPR). The experimental conditions corresponded to the adsorption under open-circuit potential. This potential is positive vs SCE and corresponds unambiguously to positive surface charge [19]. Kinetics of SPR signals after injection of  $[\text{Cu}_2\text{L}]\text{Cl}_2$  or  $[\text{Ni}_2\text{L}]\text{Cl}_2$  in water or in various supporting electrolytes are presented in Fig. 6a,b. A shift of SPR signal indicating an increase of the refraction index

near gold surface was observed in all cases. Being measured with solutions of inorganic salts, a bulk effect does not exceed 5% of the signal magnitude obtained with at the used concentrations of  $[\text{Ni}_2\text{L}]\text{Cl}_2$ ,  $[\text{Cu}_2\text{L}]\text{Cl}_2$  or  $[\text{Ni}_2\text{L}]\text{Cl}_2$  replacement by the background solution resulted in desorption of the reactants from the surface (Figs. 6c,d) and decrease of the SPR signal to the level of the background response. The data in Fig. 6 confirm a strong reversible adsorption of the complexes on the gold support.

To estimate a surface coverage ( $\theta$ ), we fitted the experimental data for several concentrations of  $[\text{Ni}_2\text{L}]\text{Cl}_2$  ( $c$ ) to Frumkin isotherm (Eq. 7) (Fig. 7) under an assumption that experimental SRP signal does not obligatory reach the value corresponding to the actual limiting surface coverage ( $R_{\text{max}}$ ). The best fit is obtained for  $R_{\text{max}}$  being in 1.4 time higher than maximum observable SPR signal for the highest concentration in concentration range of 0.1–1 mM. We got the isotherm parameters  $a = -1.5$  and  $B = 1.7 \cdot 10^4 \text{ M}^{-1}$  (Fig. 6). This result can be considered as a rough estimation; however, it indicates that the surface coverage on gold under open circuit is essentially lower as compared to mercury (at negative electrode charges). To make fitting more reliable, we used the relations of the parameters  $a$  and  $B$  to parameters of adsorption–desorption kinetics and involved independent data on SPR transients. Frumkin isotherm is consistent with the following kinetic equations for adsorption and desorption:

$$v_{\text{ads}} = k_{\text{ads}} \cdot c(1 - \theta) \cdot e^{\alpha\theta} \quad (8)$$

$$v_{\text{des}} = k_{\text{des}} \cdot \theta \cdot e^{-\beta\theta} \quad (9)$$

Taking into account the equilibrium conditions  $v_{\text{ads}} = v_{\text{des}}$  and Eq. 7 it gives Eqs. 10 and 11:

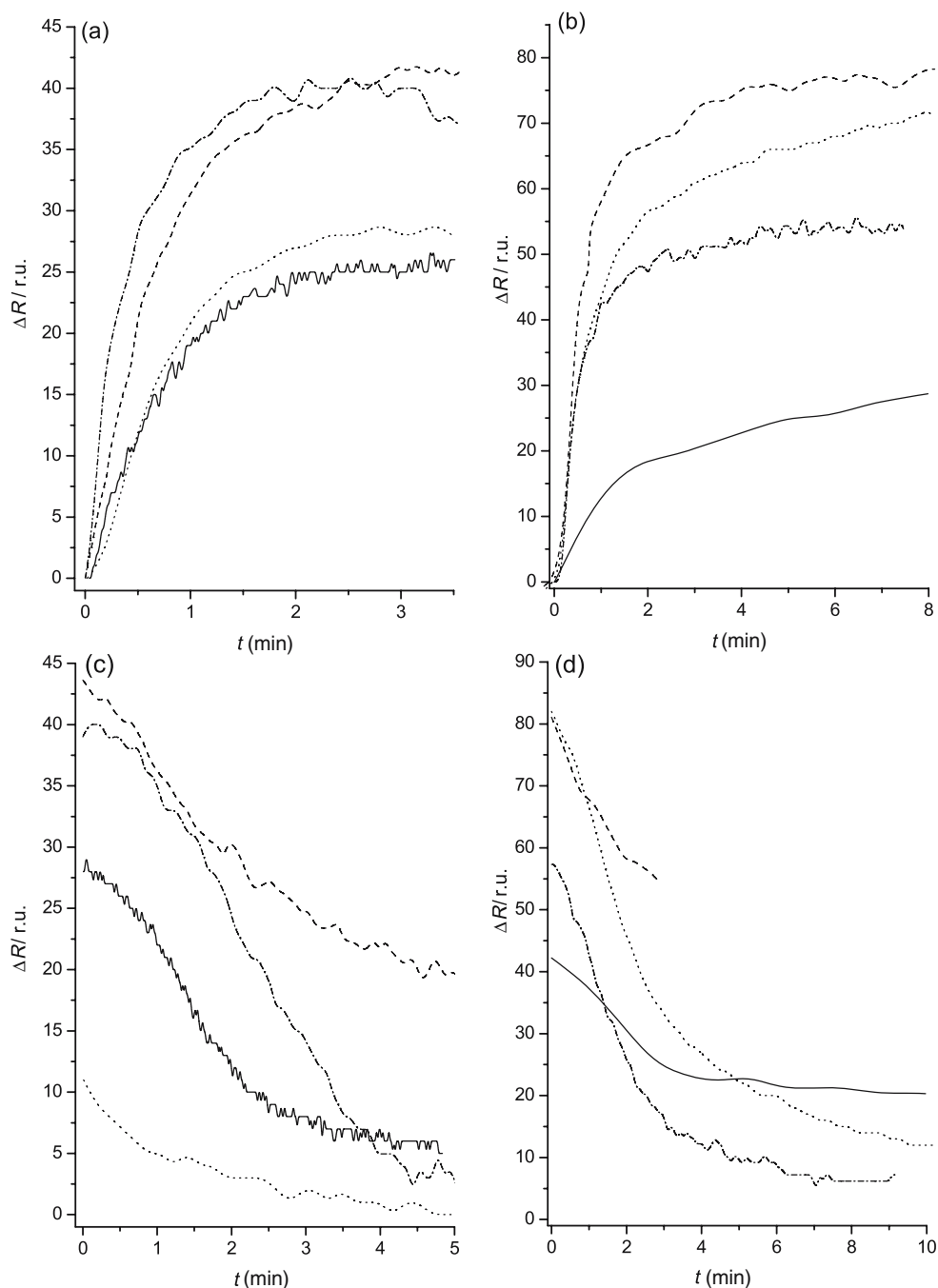
$$B = \frac{k_{\text{ads}}}{k_{\text{des}}} \quad (10)$$

$$\alpha + \beta = 2\alpha \quad (11)$$

$V_{\text{des}}$ ,  $\theta$ -dependence presented by Eq. 9 was fitted to experimental desorption curves for various concentrations of  $[\text{Ni}_2\text{L}]\text{Cl}_2$  (pH 4.7 acetate buffer). All the curves in the concentration range from 0.001 to 1 mM can be satisfactorily fitted with  $\beta = 0.01$  and  $k_{\text{des}} = 0.007 \text{ s}^{-1}$ . The possibility of desorption process to interfere with adsorption was taken into account when the adsorption curves were treated, i.e., SPR signal of adsorption transients was assumed to be  $k_{\text{ads}} \cdot c(1 - \theta) \cdot e^{\alpha\theta} - k_{\text{des}} \cdot \theta \cdot e^{-\beta\theta}$ . For the concentrations from 0.1 to 1 mM the fitting gives  $\alpha = -3$  and  $k_{\text{ads}} = 6.5 \cdot 10^3 \text{ M}^{-1} \text{ min}^{-1}$ .

The rate constants of  $[\text{Ni}_2\text{L}]\text{Cl}_2$  adsorption and desorption ( $k_{\text{ads}}$  and  $k_{\text{des}}$ ) are lower than those pointed in the literature

**Fig. 6** SPR curves of adsorption and desorption of 0.1 mM  $[\text{Cu}_2\text{L}]\text{Cl}_2$  (a and c) and  $[\text{Ni}_2\text{L}]\text{Cl}_2$  (b and d) onto gold support from  $\text{H}_2\text{O}$  (solid line), 0.1 M NaCl (dotted line), 0.05 M acetate buffer pH 6.0 (dashed line), pH 4.7 (dash-dotted line)



for protein adsorption and desorption  $k_{\text{ads}} \sim 10^7 \text{ M}^{-1} \text{ min}^{-1}$  and  $k_{\text{des}} \sim 1 \text{ min}^{-1}$  ( $B \sim 10^7 \text{ M}^{-1}$ ) [20]. Estimation of  $a$  and  $B$  from  $k_{\text{ads}}$ ,  $k_{\text{des}}$ ,  $\alpha$ , and  $\beta$  using Eqs. 10 and 11 gives ca.  $-1.5$  and  $1.5 \cdot 10^4 \text{ M}^{-1}$ , correspondingly, in good agreement with the values obtained from isotherms. Consequently, it is possible to find self-consistent description of kinetic and thermodynamic adsorption data. Other adsorption isotherms (Langmuir or Temkin) were less appropriate to fit the SPR data obtained.

Considering parameter  $B$  at gold support and the dependence of  $B$  on potential at mercury electrode, it is necessary to compare potentials in a rational scale. It is

always a problem to discuss an exact value of the potential of zero charge (pzc) for polycrystalline gold. The value  $0.14\text{--}0.16 \text{ V}$  (vs NHE) reported in [19] is at the edge of pzc interval for gold single crystals ( $0.2\text{--}0.5 \text{ NHE}$  [21]). For gold wire formed under mechanic stress, any value from this interval cannot be excluded. The conditions of SPR experiment correspond to potential of open circuit that is at about  $0.6 \text{ V}$  (vs SCE). Assuming two limiting values of possible pzc, one can estimate the open-circuit potential as being in the interval of  $0.3\text{--}0.7 \text{ V}$  of the rational scale values, i.e., to rather positive electrode charge. As  $B$  value

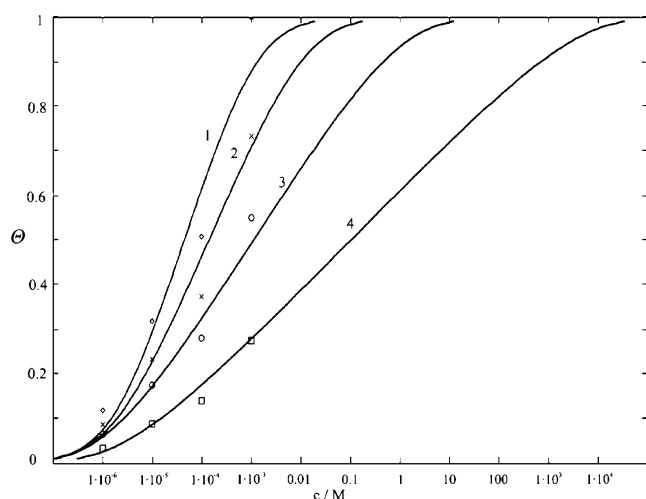


**Fig. 7** Steady state values of SPR signals for adsorption of different concentration of  $[\text{Ni}_2\text{L}]\text{Cl}_2$  (pH 4.7) corrected for saturation values (points) and calculated Frumkin isotherms (solid curves)

for this charge is close to the value found for low positive charges on mercury, the adsorption features of  $[\text{Ni}_2\text{L}]\text{Cl}_2$  at mercury and gold electrodes can be considered as similar. Simultaneously, the difference in  $a$  is pronounced, i.e., the interactions in adlayer differ strongly at negative and positive charges. A possible explanation is charge-dependent coadsorption with anions. In accordance with Fig. 6, the adsorption and desorption are quite sensitive to the nature of supporting electrolyte, but the effects are too weak for quantitative treatment. Another observation is that the adsorption of  $[\text{Cu}_2\text{L}]\text{Cl}_2$  in the presence of supporting electrolyte is slower than that of  $[\text{Ni}_2\text{L}]\text{Cl}_2$  (Fig. 6a,b). Desorption (Fig. 6c,d) is complete in both cases, but  $[\text{Cu}_2\text{L}]\text{Cl}_2$  desorption proceeds more rapidly. This difference in adsorption behavior of the complexes possibly results from the interaction of the complexes under study and coadsorbed supporting electrolyte anions.

$\text{H}_2\text{O}_2$  electrocatalysis at potentials below  $-0.2$  V corresponds to a negative gold charge, i.e., to higher surface coverage; this provides an explanation of  $[\text{Cu}_2\text{L}]\text{Cl}_2$  activity on gold in the region preceding  $[\text{Cu}_2\text{L}]\text{Cl}_2$  reduction. To discuss the difference of  $[\text{Cu}_2\text{L}]\text{Cl}_2$  and  $[\text{Ni}_2\text{L}]\text{Cl}_2$  catalytic effects on gold, we should not ignore parallel pathways (1) and (2), the former with participation of adsorbed hydroxide anions.

As the adsorption is reversible, immobilization in adlayers can hardly result in catalyst stability. One of the ways to explore catalytic features of binuclear complexes is their immobilization in 3D matrixes.

#### Immobilized $[\text{Ni}_2\text{L}]\text{Cl}_2$ and $[\text{Cu}_2\text{L}]\text{Cl}_2$

##### Polymer-modified gold electrodes

Entrapping of chemical substances in polymers is a widely used approach to immobilization. We used thin (10–100 nm)

insulating PP films obtained by oxidative electropolymerization for entrapping of  $[\text{Ni}_2\text{L}]\text{Cl}_2$  and  $[\text{Cu}_2\text{L}]\text{Cl}_2$ . The electrodes coated by pure PP films (PP–Au) and by complex-modified films ( $[\text{Cu}_2\text{L}]\text{Cl}_2$ –PP–Au) were compared.

The quantity of complexes entrapped into the film is usually not so high as in the adlayer at a mercury electrode. One can expect that the distance between  $[\text{M}_2\text{L}]\text{Cl}_2$  molecules is more than the order of the molecular diameter; it makes impossible any binding of a single  $\text{H}_2\text{O}_2$  molecule by two complex molecules simultaneously. Therefore, an observation of an essential increasing of the  $\text{H}_2\text{O}_2$  electrocatalysis rate in  $[\text{Cu}_2\text{L}]\text{Cl}_2$ –PP–Au would prove an adduct formation with a single complex molecule.

$[\text{Cu}_2\text{L}]\text{Cl}_2$  was found to lose the redox activity after entrapment into polyphenol film. This results from the cyclic voltammetry test of modified electrode in supporting electrolyte in the potential region of  $[\text{Cu}_2\text{L}]\text{Cl}_2$  reduction. Taking into account our previous conclusion concerning Eqs. 2, 3 and Eqs. 5, 6, this loss of activity should favor electrocatalysis according to Eqs. 3, 4. Catalytic currents at the potential of ca.  $-0.25$  V were registered at PP–Au and  $[\text{Cu}_2\text{L}]\text{Cl}_2$ –PP–Au electrodes (Fig. 8). After continuous potential cycling, the currents of  $\text{H}_2\text{O}_2$  reduction became constant and equal for both bare and modified electrodes.

The currents of  $\text{H}_2\text{O}_2$  reduction increase with a shift of cathodic boundary potential to negative potentials. This effect is more pronounced at bare gold electrode and less pronounced at  $[\text{Cu}_2\text{L}]\text{Cl}_2$ –PP–Au electrode. No catalytic  $\text{H}_2\text{O}_2$  reduction current was observed at pH 4.0–5.0. An increase of the concentration of supporting electrolyte results in the decrease of  $\text{H}_2\text{O}_2$  reduction current. Probably, this is caused by strong adsorption of acetate-anion and consequent prevention of  $\text{OH}_{\text{ads}}$  formation (Eq. 1).

A typical amperometric response of  $[\text{Cu}_2\text{L}]\text{Cl}_2$ –PP–Au induced by consequent additions of  $\text{H}_2\text{O}_2$  are shown in

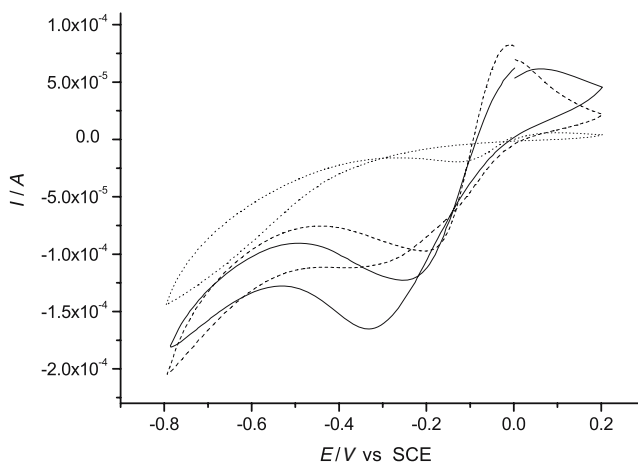


**Fig. 8** Cyclic voltammograms in 0.01 M acetate buffer solution pH 6.0+14 mM  $\text{H}_2\text{O}_2$  at blank gold wire electrode (dotted line), gold modified by (dashed line) polyphenol, (solid line) polyphenol with  $[\text{Cu}_2\text{L}]\text{Cl}_2$ , (the third scans are presented) scan rate 50 mV/s



Fig. 9 (insert). Response time of both modified and bare electrodes is within 10–20 s interval and close to the data reported in [22] (20–30 s). Then, the current becomes constant till the next aliquot of H<sub>2</sub>O<sub>2</sub> was added.

We attempted also to study an effect of phenol/[Cu<sub>2</sub>L]Cl<sub>2</sub> ratio in polymerization solution on the electrochemical response of modified electrodes to H<sub>2</sub>O<sub>2</sub>. According to Fig. 9, the maximum response of [Cu<sub>2</sub>L]Cl<sub>2</sub>-PP-Au electrode is observed if polymerization solution contains 0.5 mM [Cu<sub>2</sub>L]Cl<sub>2</sub> and 3 mM phenol. Freshly prepared films ([Cu<sub>2</sub>L]Cl<sub>2</sub>-PP-Au) demonstrated more intensive signal than that of PP-Au and much more than the signals observed at bare gold electrode.

The dependence of amperometric response of both modified and bare electrodes (at -0.6 V) on H<sub>2</sub>O<sub>2</sub> concentration is linear. The sensitivity of detection increases in the row: bare gold electrode < PP-Au < [Cu<sub>2</sub>L]Cl<sub>2</sub>-PP-Au electrode. The response of [Cu<sub>2</sub>L]Cl<sub>2</sub>-PP-Au electrode at -0.6 V is stable for 60 min, then in the next 40 min, a 40% decrease of the response occurs.

The amperometric experiments show the prospects of sensing applications, i.e., the possibility of H<sub>2</sub>O<sub>2</sub> determination at PP-Au or [Cu<sub>2</sub>L]Cl<sub>2</sub>-PP-Au electrodes at rather negative potentials (ca. -0.6 V). In comparison to platinum electrode coated by polymerized tyrosine [22], the [Cu<sub>2</sub>L]Cl<sub>2</sub>-PP-Au exhibit electrocatalytic activity of H<sub>2</sub>O<sub>2</sub> oxidation at much lower anodic potential. Generally, the use of negative potentials in amperometric sensors has some advantages to avoid an interference with other species in analytic signal or to provide mild conditions for other sensor components.

**Fig. 9** The effect of [Cu<sub>2</sub>L]Cl<sub>2</sub> concentration in polymerization solution on amperometric signal (at -0.4 V) in acetate buffer pH 6.0+(curve 1) 1.38, (2) 1.04, (3) 0.7, and (4) 0.46 mM H<sub>2</sub>O<sub>2</sub>. The current density of bare gold electrode under the same conditions is 44, 34, 21, and 6 mkA/sm<sup>2</sup>. *Insert* amperometric signal at PP-[Cu<sub>2</sub>L]Cl<sub>2</sub>-modified gold electrode after consequent addition of 1.38, 1.55, 1.71, 1.88, 2.04, 2.35, and 2.67 mM H<sub>2</sub>O<sub>2</sub> (at -0.4 V)

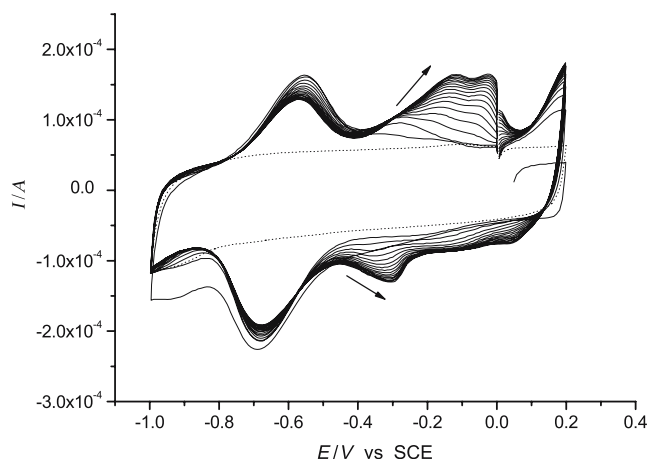
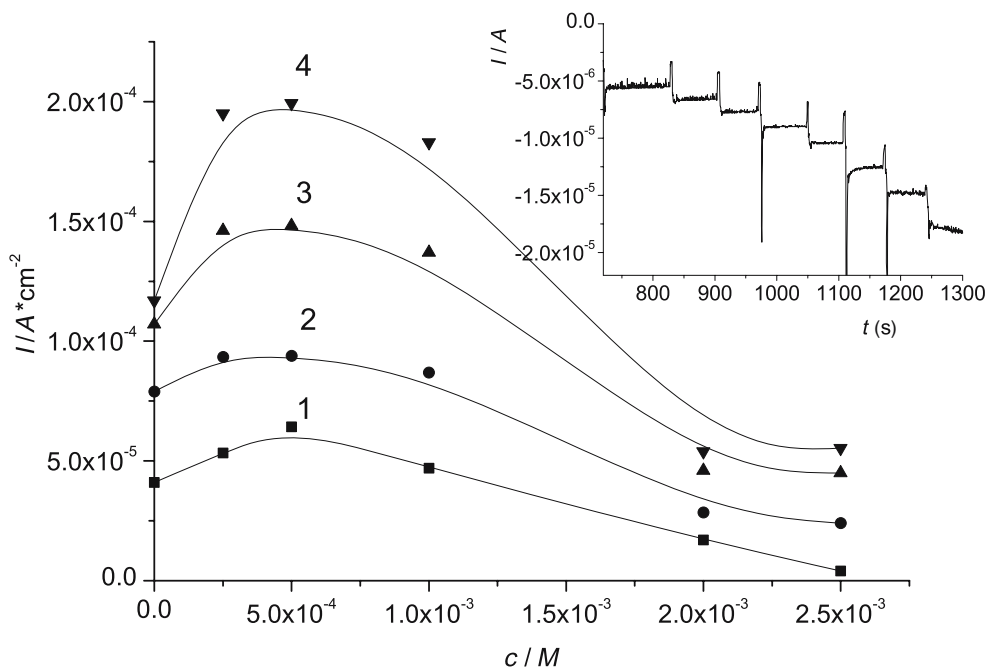


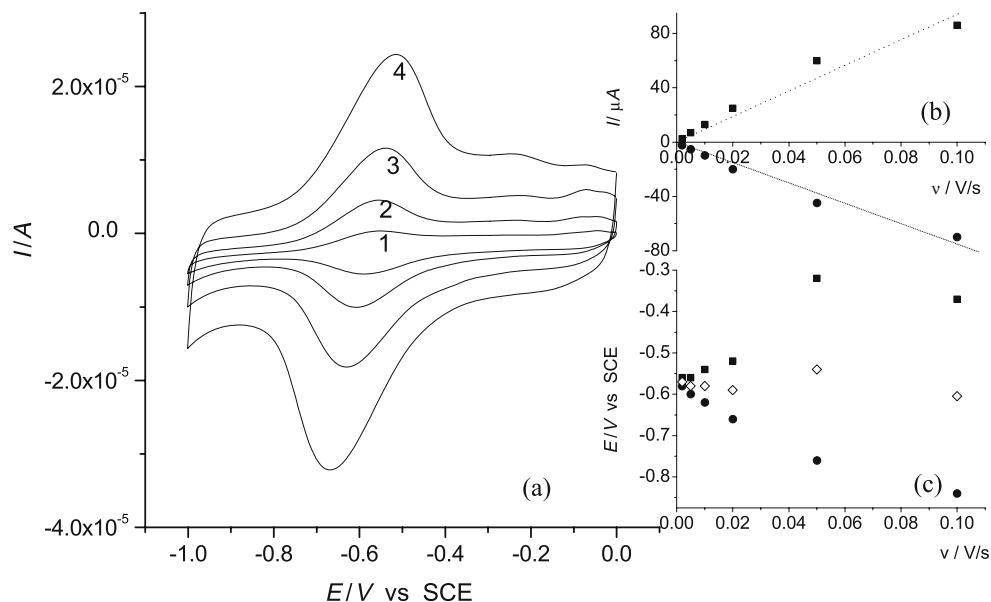
**Fig. 10** Cyclic voltammograms (solid lines) of CPE with [Cu<sub>2</sub>L]Cl<sub>2</sub> (prepared by procedure 2), (dotted line) bare CPE in 0.1 M acetate buffer solution pH 6.0, scan rate 50 mV/s. Arrows denote the evolution of the curves shape in the course of consequent cycling (from first to forty-second)

*Carbon paste electrodes*

A reversible redox conversion of [Cu<sub>2</sub>L]Cl<sub>2</sub> was revealed earlier in adlayer at HOPG surface [10]. Though this process was interfered with irreversible reduction of dissolved [Cu<sub>2</sub>L]Cl<sub>2</sub> species, it was consistent with the hypothesis of “reversible demetallation” [22].

A more pronounced reversibility of [Cu<sub>2</sub>L]Cl<sub>2</sub> reduction was detected by cyclic voltammetry after incorporation of [Cu<sub>2</sub>L]Cl<sub>2</sub> into CPE. This approach is often used to study electrochemistry of poorly soluble reactants or some organic compounds [23]. Certain electrochemical responses

**Fig. 11** **a** Cyclic voltammograms of CPE with  $[\text{Cu}_2\text{L}]\text{Cl}_2$  (prepared by procedure 1) in 0.05 M acetate buffer solution pH 6.0, scan rates (1) –2, (2) –5, (3) –10, (4) –20 mV/s. **b, c** Dependence of **(b)** peak currents (*squares* anodic; *circles* cathodic) and formal potential (*rhombs*) on scan rate from data at Fig. 10a



of the CPE electrodes are found to depend on the preparation procedure, i.e., on the type of solvents in use, on the duration, and the way of drying.

Voltammogram of CPE prepared by procedure 2 and containing  $[\text{Cu}_2\text{L}]\text{Cl}_2$  (solid curve, Fig. 10) demonstrates the reversible redox feature (formal potential  $E_f$  is  $-0.62$  V) absent from the response of a blank CPE in the same solution (dotted curve, Fig. 10). Consequent cycling of potential results in appearance of additional peaks at more positive potentials. The similar peaks were observed earlier at  $[\text{Cu}_2\text{L}]\text{Cl}_2$  reduction at glassy carbon and highly oriented pyrographite electrodes at pH 6 [10]. These peaks are associated with chemically irreversible  $[\text{Cu}_2\text{L}]\text{Cl}_2$  reduction resulting in metallic copper formation and its desorption (oxidation).

Long-term stability of the reversible redox feature can be achieved by using procedure 1 and decreasing the anodic potential limit. For both procedures, the decrease of the anodic potential limit favors higher stability. This is illustrated by Fig. 11a. The voltammograms of CPE with  $[\text{Cu}_2\text{L}]\text{Cl}_2$  prepared by procedure 1 show a redox couple at  $E_f -0.58$  V. Additional weakly pronounced anodic and cathodic peaks appear at ca. 0.2 and  $-0.2$  V, respectively, if the potential is cycled up to more positive values, but no current increase in consequent scans is observed for these additional features.

The voltammetric analysis showed a linear dependence of peak currents ( $I_{pc}$  and  $I_{pa}$ ) and potentials ( $E_{pc}$  and  $E_{pa}$ ) on scan rate from 0.002 to 0.1 V/s (Fig. 11b and c). The  $I_{pc}/I_{pa}$

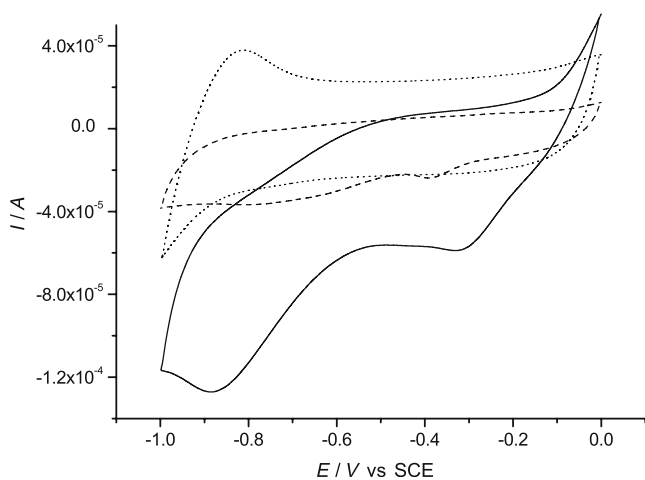


**Fig. 12** Cyclic voltammograms for reduction of 5 mM  $\text{H}_2\text{O}_2$  in 0.05 M acetate buffer solution pH 6.0 at blank CPE (dashed line) (prepared by procedure 1), at CPE with  $[\text{Ni}_2\text{L}]\text{Cl}_2$  (solid line); a response of CPE with  $[\text{Ni}_2\text{L}]\text{Cl}_2$  in 0.05 M acetate buffer solution pH 6.0 (dotted line), scan rate 50 mV/s

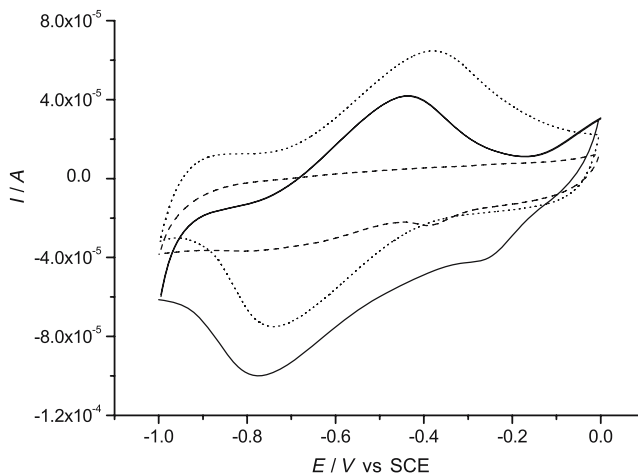


**Fig. 13** Cyclic voltammograms for reduction of 5 mM  $\text{H}_2\text{O}_2$  in 0.05 M acetate buffer solution pH 6.0 at blank carbon paste electrode (dashed line), at CPE with  $[\text{Cu}_2\text{L}]\text{Cl}_2$  (prepared by procedure 1) (solid line); a response of CPE with  $[\text{Cu}_2\text{L}]\text{Cl}_2$  in 0.05 M acetate buffer solution pH 6.0 (dotted line), scan rate 50 mV/s

ratio is close to 1 at slow scan rates and deviates from 1 at scan rates higher than 0.02 V/s (Fig. 11b). The difference ( $E_{pa} - E_{pc}$ ) decreases with the scan rate and does not exceed 0.01–0.02 V upon extrapolation of scan rate to zero (Fig. 11c). No dramatic shift of  $E_f$  is observed with variation of scan rate (Fig. 11c). In accordance with criteria of cyclic voltammetric analysis [24], the signals of CPE modified with  $[Cu_2L]Cl_2$  result from redox conversion of  $[Cu_2L]Cl_2$  in solid or adsorbed state.

One cannot exclude incomplete evaporation of organic solvent from the paste during the CPE preparation. Therefore, the  $[Cu_2L]Cl_2$  crystals can be partly dissolved and consequently adsorbed at carbon particles. In this case, a redox transformations of  $[Cu_2L]Cl_2$  in microcrystals and adlayers may occur. The total amount of  $[Cu_2L]Cl_2$  inserted into the paste is lower than the amount required to form a complete monolayer at the surface of carbon particles (the surface was estimated from specification of producer). The experimentally observed charge (Fig. 11a) is also lower than the charge required for redox transformation of complete monolayer of the total amount of immobilized solid. As  $[Cu_2L]Cl_2$ /carbon powder ratio does not affect the value of the charge, we assume that only a small portion of the paste located near the carbon paste–gold support boundary, undergoes redox transformation. Under these circumstances, the complete coverage of carbon particles by  $[Cu_2L]Cl_2$  at this boundary layer cannot be excluded.

Due to fabrication details, CPEs prepared by procedure 2 are expected to be more porous. The prolonged cycling of their potential affects the electroreduction of  $[Cu_2L]Cl_2$  in the same way as the addition of water to aprotic solvent (Glukhov et al., in preparation). According to the literature data,  $[Cu_2L]Cl_2$  is involved in two-step one-electron reduction in aprotic solvents. If water-containing media are used, the source of protons results in more completed and chemically irreversible  $[Cu_2L]Cl_2$  reduction. Hence, the evolution of voltammograms in consequent scans presented in Fig. 10 can be explained by the protonation effect, if CPE are considered as initially aprotic medium.

The onset of  $[Ni_2L]Cl_2$  reduction peak in CPE is observed at more negative potential than  $-0.9$  V (dotted curve in Fig. 12) with coupled oxidation peak at  $-0.85$  V. More complete reduction of  $[Ni_2L]Cl_2$  is difficult to observe because it would be hindered by background redox process while scanning in more broad potential window. Despite of this limitation, there are no doubts in  $[Ni_2L]Cl_2$  redox activity in CPE.

To summarize, Robson type complexes are entrapped into carbon paste electrode either in the form of adsorbate or as a solid, and demonstrate the reversible redox behavior if aqueous solution is not accumulated inside CPE.

These CPEs, modified by  $[Cu_2L]Cl_2$  and  $[Ni_2L]Cl_2$ , were tested for electrocatalytic effect of  $H_2O_2$  reduction.

According to Fig. 13, the voltammogram of  $H_2O_2$  reduction at CPE modified with  $[Cu_2L]Cl_2$  (solid line) is very similar to a superposition of curves for a blank CPE in  $H_2O_2$  solution (dashed line) and CPE with  $[Cu_2L]Cl_2$  in acetic buffer (dotted line). That is, no catalytic effect of  $[Cu_2L]Cl_2$  is observed at CPE.

Noticeable amplification of  $H_2O_2$  reduction currents is observed at the voltammograms recorded at CPE with  $[Ni_2L]Cl_2$  (Fig. 12). In comparison with cyclic voltammogram of bare CPE in  $H_2O_2$  (dashed line) and redox signals of CPE with  $[Ni_2L]Cl_2$  in the absence of  $H_2O_2$  (dotted line), solid curve exhibits two irreversible reduction peaks at ca.  $-0.3$  and  $-0.9$  V. Both of the peak current values exceed the total current at bare CPE voltammogram (dashed line) and background response of CPE with  $[Ni_2L]Cl_2$  (dotted line). Thus, only  $[Ni_2L]Cl_2$  but not  $[Cu_2L]Cl_2$  reveals catalytic effect on  $H_2O_2$  reduction similarly to the effect of  $[Ni_2L]Cl_2$  adlayer on mercury electrode.

## Conclusions

An increase of hydrogen peroxide reduction current is found at different systems containing  $[Ni_2L]Cl_2$  and  $[Cu_2L]Cl_2$ :  $[Ni_2L]Cl_2$  adlayer at mercury electrode,  $[Ni_2L]Cl_2$  and  $[Cu_2L]Cl_2$  at gold electrode,  $[Cu_2L]Cl_2$ -polyphenol film gold electrode,  $[Ni_2L]Cl_2$ . As electrocatalytic activity is not observed if a reduction of central ions in  $[M_2L]Cl_2$  takes place, the catalytic effect of the systems on  $H_2O_2$  electroreduction is associated with the ability of  $[M_2L]Cl_2$  to form an adduct with  $H_2O_2$ . The suggested dependence of  $[M_2L]Cl_2$  adsorbate reactivity on metal–metal distance is confirmed by comparison of possible geometry of catalytically active layers in these relative systems. The optimal distance of ca. 4 Å is consistent with the literature data on oxygen electrocatalysis by metalloporphyrin dimer via adduct formation [6, 4].

**Acknowledgements** DAAD (German Academic Exchange Service) is acknowledged for the fellowship of N. Roznyatovskaya. This study is also supported partially by the Russian Foundation for Basic Research (grant 05-03-32 381a). We are grateful to the synthesis group of laboratory of Prof. Yu. A. Ustynyuk for providing us with reactants.

## References

1. Zagal JH (1992) *Coord Chem Rev* 119:89
2. Yeager E (1984) *Electrochim Acta* 29:1527
3. Collman JP, Marocco M, Denisevich P, Koval C, Anson FC (1979) *J Electroanal Chem* 101:717
4. Duran RR, Bencosme CS, Collman JP, Anson FC (1983) *J Am Chem Soc* 105:2710
5. Marcuccio SM, Svirskaya PI, Greenberg S, Lever ABP, Leznoff CC, Tomer KB (1985) *Can J Chem* 63:3057

6. Costa G, Tavagnacco C, Balducci G (1991) *J Electroanal Chem* 318:183
7. Gagne RR, Koval CA (1979) *J Am Chem Soc* 101:4571
8. Aono T, Wada H, Yonemura M, Ohba M, Okawa H, Fenton DE (1997) *J Chem Soc Dalton Trans*:1527
9. Roznyatovskaya NV, Tsirlina GA, Roznyatovskii VV, Mitiaev AS, Smurnyy YD (2005) *Mendeleev Commun* 15(3):93
10. Roznyatovskaya NV, Vassiliev SYu, Yusipovich AI, Tsirlina GA, Roznyatovskii VV (2005) *J Solid State Electrochem* 9:581
11. Roznyatovskaya NV, Tsirlina GA, Roznyatovskii VV, Reshetova MD, Ustynuyk YuA (2004) *Russ J Electrochem* 40(9): 955
12. Long DD, Marx KA, Zhou T (2001) *J Electroanal Chem* 501:107
13. Pilkington NH, Robson R (1970) *Aust J Chem* 23:2225
14. Damaskin BB, Petrii OA, Batrakov BB (1968) Adsorption of organic substances on electrodes. Nauka, Moscow, p 70 (in Russian)
15. Astakhov II, Grafov BM, Kabanov BN et al (1981) Kinetics of complex reactions. Nauka, Moscow, p 122 (in Russian)
16. Bocris JO, Oldfield LF (1955) *Trans Faraday Soc* 51:249
17. Matsumoto F, Uesugi S, Koura N, Ohsaka T (2003) *J Electroanal Chem* 549:71
18. Van Den Brink F, Visscher W, Barendrecht E (1983) *J Electroanal Chem* 157:305
19. Wegner GJ, Wark AW, Lee HJ, Codner E, Saeki T, Fang S, Corn RM (2004) *Anal Chem* 76:5677
20. Zelinskii AG, Bek RYu, Makurin AL, Abdulov CD (1978) *Russ J Electrochem* 14:1740 (in Russian)
21. Hamelin A, Vitanov T, Sevastianov E, Popov A (1983) *J Electroanal Chem* 145:225
22. Marken F, Cromie S, McKee V (2003) *J Solid State Electrochem* 7:141
23. Kalcher K, Kauffmann J-M, Wang J, Švancara I, Vytr'as K, Neuhold C, Yang Z (1995) *Electroanalysis* 7(1):5
24. Bard AJ, Faulkner LR (2001) *Electrochemical methods. Fundamentals and applications*. Wiley-VCH, Weinheim, pp 1–856